FLOW OF AN ELECTRICALLY CONDUCTING FLUID OVER A FLAT PLATE IN A PERPENDICULAR MAGNETIC FIELD

B. Ya. Gurevich, R. L. Miller, A. B. Tsinober, and A. G. Shtern

Magnitnaya Gidrodinamika, Vol. 2, No. 4, pp. 69–77, 1966

UDC 538.4

The boundary layer of an electrically conducting fluid over a flat plate in the presence of a perpendicular magnetic field is investigated.

In the first part of the study analytical solutions are found by two methods: an integral method and a series solution which converges at arbitrary values of the Stuart number. The series solution was found to converge to the exact solution which represents the asymptotic behavior of the boundary layer. The first few terms of the series are sufficient for an accurate representation of the velocity profile at any Stuart number. Numerical calculations have also been performed.

In the second part of the paper the experimental measurement of the velocity distribution in the boundary layer is described.

The analysis of the results is given in the third part of the paper.

1. We shall consider the two-dimensional boundary layer flow over a semi-infinite flat plate. The flow is uniform at upstream infinity; the velocity is parallel to the surface of the plate; the magnetic field is perpendicular to the flow; the electric currents are assumed to vanish at upstream infinity, i.e., the undisturbed flow does not interact with the magnetic field. Using the usual notation the boundary layer equations can be written for this case in the following form:

$$u\frac{\partial u}{\partial x}+v\frac{\partial u}{\partial y}=\nu\frac{\partial^2 u}{\partial y^2}+\frac{\sigma B^2}{\rho}(u_0-u);$$

$$\frac{\partial u}{\partial x}+\frac{\partial v}{\partial y}=0 \qquad (1)$$

with the boundary conditions

$$u(x,0)=v(x,0)=0;\quad u(x,\infty)=u_0; \qquad (2a)$$

$$u(0,y)=u_0;\quad v(0,y)=0. \qquad (2b)$$

New variables are defined:

$$\xi=\frac{\sigma B^2}{\rho u_0}x;\quad \eta=\sqrt{\frac{\sigma B^2}{\rho\nu}}y \qquad (3)$$

(obviously, these variables can be introduced only if $B \neq 0$);

$$\bar{v}=v\sqrt{\frac{\rho}{\sigma B^2\nu}};\quad \bar{u}=\frac{u}{u_0}.$$

Equation (1) can be rewritten in the following form:

$$\bar{u}\frac{\partial\bar{u}}{\partial\xi}+\bar{v}\frac{\partial\bar{u}}{\partial\eta}=\frac{\partial^2\bar{u}}{\partial\eta^2}+1-\bar{u};\quad \frac{\partial\bar{u}}{\partial\xi}+\frac{\partial\bar{v}}{\partial\eta}=0, \qquad (4)$$

with the boundary conditions

$$\bar{u}(\xi,0)=\bar{v}(\xi,0)=0;\quad \bar{u}(\xi,\infty)=1; \qquad (5a)$$

$$\bar{u}(0,\eta)=1;\quad \bar{v}(0,\eta)=0. \qquad (5b)$$

Combining the two equations in Eq. (4) we obtain

$$\frac{\partial}{\partial\xi}\{\bar{u}(1-\bar{u})\}+\frac{\partial}{\partial\eta}\{\bar{v}(1-\bar{u})\}=-\frac{\partial^2\bar{u}}{\partial\eta^2}-1+\bar{u}. \qquad (6)$$

Since (4) has an exact solution

$$\bar{u}=1-e^{-\eta};\quad \bar{v}=0, \qquad (7)$$

the magnetohydrodynamic boundary layer behaves asymptotically as $\xi \to +\infty$. Thus we shall seek a solution $\bar{u}(\xi,\eta)$ of the form:

$$\bar{u}=1-e^{-\eta/\delta(\xi)}. \qquad (8)$$

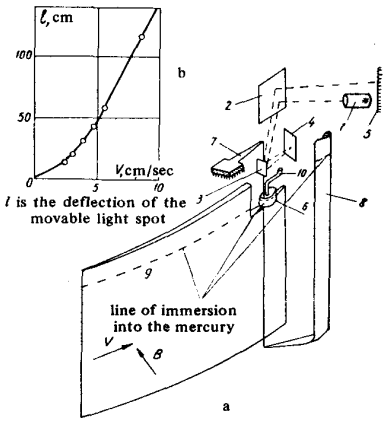

Fig. 1. Experimental apparatus (a) and calibration curve (b).

If one integrates (6) with respect to η from 0 to ∞, the following equation is obtained for $\delta(\xi)$:

$$\tfrac{1}{2}\delta'=1/\delta-\delta,$$

whose integral yields

$$\delta=(1-Ce^{-4\xi})^{1/2}.$$

The constant of integration is found from the condition $\bar{u}(0, \eta) = 1$: C = −1. Hence the final solution is

$$\delta = (1-e^{-4\xi})^{1/2}; \quad \bar{u} = 1-\exp(-\eta/\sqrt{1-e^{-4\xi}}) \qquad (9)$$

or in physical variables

$$u = u_0[1-\exp(-M_y/\sqrt{1-e^{-4N_x}})], \qquad (10)$$

where M_y is the Hartmann number based on the y coordinate, and N_x is the Stuart number based on the x coordinate.

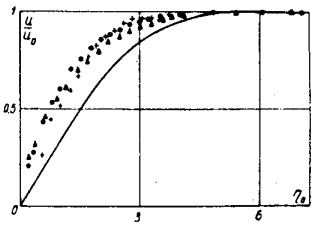

Fig. 2. Comparison of the measurements with the Blasius curve. ●: Re = 51 000, +: Re = = 56 000 (the measurements were performed by the authors); ▲: results corrected for the effect of the magnetic field upon the resistance of the fiber during the calibration.

The friction coefficient of a plate of length x is found to be

$$C_f = \frac{1}{M_x}\ln(1+\sqrt{1-e^{-4N_x}}) + \frac{2M_x}{\mathrm{Re}_x}. \qquad (11)$$

If $N_x = 0$ (and thus $M_x = 0$), the velocity profile is given by

$$\bar{u} = 1-e^{-\eta/2}, \quad \eta = y/\sqrt{x},$$

and the corresponding friction coefficient is

$C_f = 2/\sqrt{\mathrm{Re}_x}$ (the Blasius solution yields $1.328/\sqrt{\mathrm{Re}_x}$).

It is noteworthy that the velocity defined by (8) increases monotonically towards the edge of the boundary layer contrary to profiles described by fourth order polynomials, where it changes nonmonotonically at sufficiently large N_x values [1].

We shall seek now a series solution to the boundary layer equations. For this purpose we introduce a stream function and consider the boundary layer equation in the following dimensionless form:

$$\frac{\partial\psi}{\partial y}\frac{\partial^2\psi}{\partial x\partial y} - \frac{\partial\psi}{\partial x}\frac{\partial^2\psi}{\partial y^2} = \frac{\partial^3\psi}{\partial y^3} + N\left(1-\frac{\partial\psi}{\partial y}\right) \qquad (12)$$

with the boundary conditions

$$\psi(x, 0) = \frac{\partial\psi(x, 0)}{\partial y} = 0, \quad \frac{\partial\psi(x, \infty)}{\partial y} = 1, \qquad (13)$$

where $N = \sigma B^2\nu/\rho u_0^2$, and ν/u_0 is chosen for characteristic length. The coordinate is replaced by a new variable whose form is suggested by (10):

$$\eta = yN^{1/2}(1-e^{-Nx})^{-1/2}.\dagger$$

We seek a solution to (12) subject to the boundary conditions (13) in the form of fnfinite series

$$\psi = N^{-1/2}(1-e^{-Nx})^{1/2}\sum_{n=0}^{\infty}\varphi_n(\eta)e^{-nNx}. \qquad (14)$$

Substituting Eq. (14) into Eq. (12) and observing that

$$\frac{\partial\eta}{\partial y} = N^{1/2}(1-e^{-Nx})^{-1/2}; \quad \frac{\partial\eta}{\partial x} = -\frac{Ne^{-Nx}}{2(1-e^{-Nx})}\eta,$$

we obtain the expression

$$-\sum_{n=0}^{\infty}\varphi_n'(\eta)z^nN\sum_{n=0}^{\infty}n\varphi_n'(\eta)z^n - \sum_{n=0}^{\infty}\varphi_n'(\eta)z^n\frac{\eta zN}{2(1-z)}\times$$
$$\times\sum_{n=0}^{\infty}\varphi_n''(\eta)z^n - \frac{zN}{2(1-z)}\sum_{n=0}^{\infty}\varphi_n''(\eta)z^n\sum_{n=0}^{\infty}\varphi_n(\eta)z^n +$$
$$+\sum_{n=0}^{\infty}\varphi_n''(\eta)z^n\sum_{n=0}^{\infty}nN\varphi_n(\eta)z^n + \frac{\eta Nz}{2(1-z)}\sum_{n=0}^{\infty}\varphi_n''(\eta)z^n\times$$
$$\times\sum_{n=0}^{\infty}\varphi_n'(\eta)z^n = \frac{N}{1-z}\sum_{n=0}^{\infty}\varphi_n'''(\eta)z^n + N -$$
$$-N\sum_{n=0}^{\infty}\varphi_n'(\eta)z^n, \qquad (15)$$

where $z = e^{-Nx}$.

Equating the coefficients of the terms containing equal powers of z we obtain equations defining the functions $\varphi_n(\eta)$.

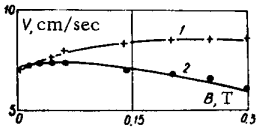

Fig. 3. Upstream of flow velocity as a function of the magnetic field strength for conducting and nonconducting plates. 1) plastic plate; 2) stainless steel plate.

The function $\varphi_0(\eta)$ is defined by

$$\varphi_0''' - \varphi_0' + 1 = 0 \qquad (16)$$

†It is noted that the product Nx is identical with the Stuart number N_x based on the physical length of the plate.

with the boundary conditions

$$\varphi_0(0)=\varphi_0'(0)=0, \quad \varphi_0'(\infty)\doteq 1. \tag{17}$$

For $\varphi_1(\eta)$ we get

$$\varphi_1'''+(\varphi_0-1)\varphi_1'-\varphi_0''\varphi_1+\frac{1}{2}\varphi_0\varphi_0''+\varphi_0'-1=0 \tag{18}$$

with the boundary conditions

$$\varphi_1(0)=\varphi_1'(0)=\varphi_1'(\infty)=0. \tag{19}$$

In general, for the $\varphi_n(\eta)$ function ($n \geq 2$) we obtain

$$\varphi_n'''+(n\varphi_0'-1)\varphi_n'-n\varphi_0''\varphi_n=-\varphi_{n-1}'-\frac{1}{2}\varphi_0''\varphi_{n-1}-$$

$$-\sum_{k=0}^{n-2}\left\{\frac{1}{2}\varphi_k\varphi_{n-k-1}''+(k+1)\varphi_{k+1}(\varphi_{n-k-2}''-\varphi_{n-k-1}'')+\right.$$

$$\left.+(k+1)\varphi_{k+1}'(\varphi_{n-k-1}'-\varphi_{n-k-2}')\right\}, \tag{20}$$

with

$$\varphi_n(0)=\varphi_n'(0)=\varphi_n'(\infty)=0.$$

Equation (16) and the boundary conditions (17) are satisfied by the solution

$$\varphi_0(\eta)=-1+\eta+e^{-\eta}, \tag{21}$$

while the solution corresponding to (18) and the boundary conditions (19) is

$$\varphi_1(\eta)=-\frac{1}{2}+\left(\frac{1}{2}+\frac{1}{2}\eta\right)e^{-\eta}, \tag{22}$$

and, in general, for $\varphi_n(\eta)$ we obtain

$$\varphi_n(\eta)=-\frac{(2n)!}{2^{2n}n!\,n!}+\sum_{k=0}^{n}\frac{2(n-k)!\,\eta^k e^{-\eta}}{2^{2n-k}n!\,k!\,(n-k)!}; \quad n\geq 2. \tag{23}$$

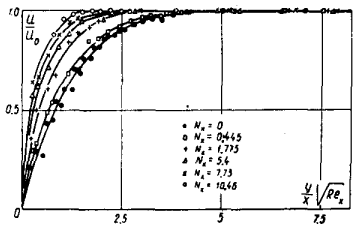

Fig. 4. Velocity profile measurements at various Stuart number values.

It can be shown by simple means that the series corresponding to ψ and all its derivatives are uniformly convergent within the interval $\{0 \leq x < \infty,\ 0 \leq \eta < \infty\}$.

It also can be shown that series (14) converges to the asymptotic solution

$$\psi=y+\frac{1}{\sqrt{N}}(e^{-\sqrt{N}y}-1) \tag{24}$$

at any Nx value.

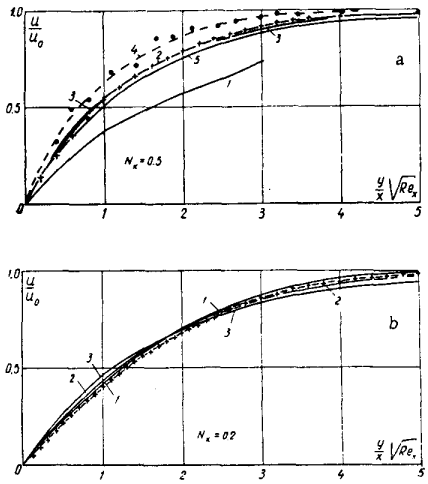

Fig. 5. Comparison of the measurements with calculated profiles. +: numerical calculations, 1) by Rossow's method, 2) by the first three terms of series (14), 3) by Eq. (10), 4) experimental measurements with N_X = 0.445, 5) asymptotic profile.

Hence the function (24) written in the form

$$\psi=\eta(1-e^{-Nx})^{1/2}+N^{-1/2}\{\exp[-\eta(1-e^{-Nx})]-1\}$$

is the generating function for the system (23). Furthermore, since the functions (23) in series (14) are obtained from Eq. (12), and the variable η is chosen so that with Nx = 0 it reduces to the well-known Blasius variable it is expected that the first few terms of series (12) yield a sufficiently accurate solution at any value of the Nx parameter. As will be shown, three terms are already sufficient.

Numerical calculations based on (4) were performed for two cases:

1) for the case represented by the boundary conditions (5a) and (5b),

2) for the case where (5b) is replaced by $\bar{u}(0,\eta) = f(\eta)$, where $f(\eta)$ is the Blasius profile based on the η variable and corresponding to $Re_X = u_0x/\nu = 0.3553$.

2. The velocity profile measurements were carried out in an annular duct [2]. A glass fiber of d = 70–80 μ stretched parallel to the surface of the plate was used as velocity sensor. The plates were made of stainless steel or plastic and had a thickness of 2 mm, length L = 100 mm, and an active width of H = 50 mm. They had a curvature in longitudinal direction equal to that of the duct; R = 240 mm.

The experimental apparatus is shown schematically in Fig. 1. A light beam emitted by light source 1 falls on the adjustable mirror 2, the reflected light proceeds to mirror 3 attached to the sensor fiber. From mirror 3 the light beam proceeds to the intermediate mirror 4 and is finally, by means of the mirror system 3 and 2, projected on the receiving screen 5.

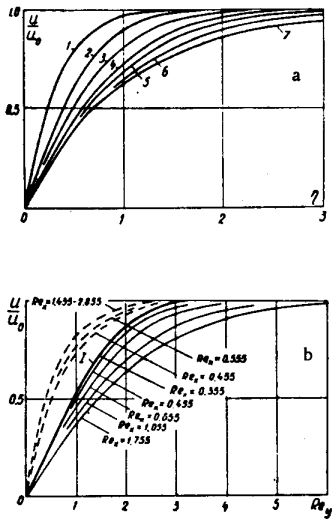

Fig. 6. Velocity profiles obtained by numerical means. a) Uniform entrance velocity: 1) $\xi = 0.01$; 2) $\xi = 0.05$; 3) $\xi = 0.1$; 4) $\xi = 0.2$; 5) $\xi = 0.3$; 6) $\xi = 0.5$; 7) $\xi = \infty$. b) Blasius profile at the entrance section. Solid lines: N = 0.2; broken lines: N = 3.

The sensor fiber led through a protective copper ring was hinged at one end to an elastic beam 7 and was connected rigidly at the other end to support 8. To adjust the parallelness and the tension of the fiber the position of beam 7 could be regulated by means of two adjusting screws not shown in this figure. A flushing solution was supplied to the protective ring through dripcock 10. The whole mechanism was mounted on a micrometer screw with a scale value of 10 μ. Hence the coordinate normal to the plate could be read with an accuracy of up to 5 μ.

During the experiments the measuring equipment was immersed in mercury until the liquid covered the entire active part of the plate and the mercury level reached the amalgamated protective ring. The protective ring was to eliminate the effect of the oxide layer on the indication of the measuring instrument and to prevent the adhesion of the fiber to the plate surface. To dissolve the oxide layer, the mercury surface was covered with a 2 to 3 mm thick layer of sulfuric acid solution (10 to 20% concentration). Within the protective ring the mercury surface was continuously flushed with the same solution by means of the dripcock. All these measures were taken to assure the reproducibility of the measurements.

The velocity sensor was calibrated after each experiment by removing the test plate from the duct. A typical calibration curve is shown in Fig. 1b. All points of this curve were taken at the maximum obtainable induction field: B = 0.3 T. This minimized the possible difference between the flow and wall velocities.

A comparison of the measurements corresponding to B = 0 with the Blasius profile is shown in Fig. 2. The Blasius variable $\eta_0 = \lim_{N \to 0} \eta$ is used as an independent variable. As can be seen, the experimental points lay much higher than the theoretical curve, i.e., the experimental velocity profile is flatter. This is apparently due to the inverse action of the boundary layer upon the main flow. Since the fluid is retarded in the boundary layers, the main flow appears to be compressed. Indeed, the plate with boundary layers on its both sides occupies about 6 to 7 mm in a 30-mm wide duct, i.e., about 20 to 25% of the total duct width. As can be seen from Figs. 3 and 4, the upstream flow is practically uniform, and thus the effect of the duct curvature is insignificant. However, it has been found that the magnetic field affects the upstream flow velocity differently if the conducting plate immersed in the flow is replaced by a nonconducting one (see Fig. 3). The e.m.f. induced in the conducting plate induces currents which find their return path through the upstream flow and produce there a retarding volume force. In the region up to B ≈ 0.05 T the velocity increases somewhat with the induction field strength, then it begins to decrease.

In conclusion we note that the effect of the magnetic field upon the friction coefficient of the sensor fiber has not been neglected. In all points where measurements were taken the Stuart number based on the fiber diameter was below 0.01 at the maximum applied field strength.

An empirical formula has been used for the estimate of the magnetic field effect*:

$$C_f/C_{f_0} = 1 + 3.4\, N_d^{1/2},$$

where C_f/C_{f0} is the ratio of the friction coefficient of a cylinder in the presence of a magnetic field to that in zero magnetic field, N_d is the Stuart number based on the fiber diameter [4].

Since the force acting on the fiber $F \sim Re^2 C_f$, and the calibration has been carried out at B = 0.3 T, the calibration curve may be corrected if one assumes that at a given velocity the signal is proportional to the force acting on the fiber. The accuracy of the calibration is limited by the accuracy of the friction coefficient which depends on the physical properties of the fluid and the dimensions of the immersed body. The correction of the velocity profile measured at B = 0

*According to the latest measurements of Kh. E. Kalis, N. M. Slyusarev, A. B. Tsinober, and A. G. Shtern [5] the formula $C_f/C_{f0} = 1 + 2.2\, N_d^{1/2}$ is more accurate in the Reynolds number range 1.5 to 200. However, we have deliberately used here a larger coefficient.

is shown in Fig. 2. As can be seen, the difference is within the limits of the measurement accuracy. Since N_d is based on a slightly higher fiber diameter (100 μ was assumed for d in our calculations), the correction thus obtained is maximum. The correction should be larger for velocity profiles measured at B = 0 than for those measured at B $\neq$ 0.

3. Figure 4 contains a family of typical experimental velocity profiles. As can be seen, as the Stuart number based on the length of the plate increases, the velocity profiles become flatter. Profiles corresponding to $N_x \geq 2$ are not much different from the asymptotic one.

Since the measurements obtained by these authors at B = 0 differ from the Blasius profile, it is not surprising that the measurements taken at sufficiently small N_x values, where the velocity profiles still differ from the asymptotic one, differ also from the theoretical values. Resistance measurements taken at $N_x = 0.445$ (our measurements taken at $N_x = 0.17$ are practically identical with those corresponding to B = 0) as well as theoretical values corresponding to $N_x = 0.5$ are shown in Fig. 5a. For the purpose of comparison the asymptotic profile is also shown in this figure. As can be seen, the profile obtained by the integral method, by the first three terms of series (14), and by numerical means are almost identical. These curves are much closer to the experimental profile than the asymptotic one. Hence, in spite of the shortcomings of our experiments, the results are sufficiently accurate.

Rossow's velocity profiles [3] are compared with those computed by the present authors in Fig. 5b. The following can be concluded about these curves. The first three terms of series (14) yield a more accurate velocity profile than the solution obtained by the integral method in the entire interval of the N_x values. The largest difference between the profiles obtained by the first three terms of Eq. (14) and the integral method is observed at N = 0, but even here it is within 7%.

Results of numerical calculations based on the solution of system (4) with the boundary conditions (5a, 5b) are shown in Fig. 6. Analogous results corresponding to a Blasius velocity profile at the entrance section are shown in Fig. 6b for two values of N (the curve calculated with $Re_x = 0.355$ corresponds to the Blasius profile). The N values where chosen in such a manner that for one of them (N = 0.2) the asymptotic profile is flatter than the entrance profile, while for the other (N = 3) the situation is reversed. Hence in the first case the profile gains curvature as Re_x increases, while in the second case it becomes flatter.

Results of wall friction calculations based on an uniform entrance velocity are shown in Fig. 7a. It is noteworthy that the curve corresponding to Rossow's method intersects the curve obtained by our numerical method at the point $N_x \cong 0.25$ where the friction is practically identical with its asymptotic value.

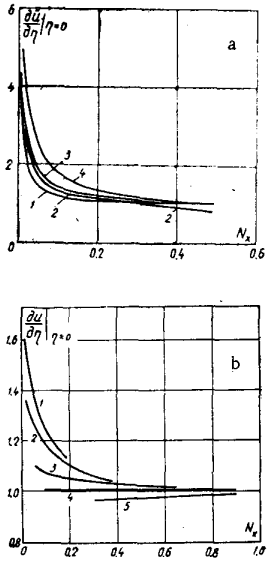

Fig. 7. Calculated wall friction. a) Uniform entrance velocity: 1) numerical calculations; 2) by Rossow's method; 3) by the first three terms of Eq. (14); 4) by Eq. (10). b) Numerical computations, Blasius profile at the entrance section. 1) N = = 0.1; 2) N = 0.2; 3) N = 0.5; 4) N = = 1; 5) N = 3.

Wall friction corresponding to a Blasius profile at the entrance section has also been computed. In this case the friction is a function of not only N_x but also of N (see Fig. 7b). As can be seen, the wall friction approaches its asymptotic value.

REFERENCES

1. A. B. Tsinober and E. V. Shcherbinin, Izv. AN LatvSSR, 6, 137, 1963.

2. G. G. Branover, I. M. Kirko, and O. A. Lielausis, "Prikladnaya magnitnaya gidrodinamika," Trudy In-ta Fizika AN LatvSSR, 12, Riga, Izd. AN LatvSSR, 167, 1961.

3. V. J. Rossow, NASA Rep. no. 1358, 1958.

4. A. B. Tsinober and E. V. Shcherbinin, Izv. AN LatvSSR, 11, 45, 1962.

5. Kh. E. Kalis, N. M. Slyusarev, A. B. Tsinober, and A. G. Shtern, Magnitnaya gidrodinamika [Magnetohydrodynamics], 4, 152, 1966.

29 June 1966